

## Electronic Supplementary Information

### **A highly transparent and photothermal composite coating as effective anti-/de-icing of glass surface**

Wei Guo,<sup>a,b</sup> Cui Liu,<sup>a,c</sup> Nian Li,<sup>a,c</sup> Min Xi,<sup>a,c</sup> Yamin Che,<sup>a,b</sup> Changlong Jiang,<sup>a,b</sup> Shudong Zhang,<sup>\* a,c</sup> and Zhenyang Wang<sup>\*a,c</sup>

*<sup>a</sup>Institute of Solid State Physics, Hefei Institutes of Physical Science, Chinese Academy of Sciences, Hefei, Anhui, 230031, China. E-mail: sdzhang@iim.ac.cn; zywang@iim.ac.cn*

*<sup>b</sup>Department of Chemistry, University of Science and Technology of China, Hefei 230026, China.*

*<sup>c</sup>Key Laboratory of Photovoltaic and Energy Conservation Materials, Hefei Institutes of Physical Science, Chinese Academy of Sciences, Hefei 230031, China.*

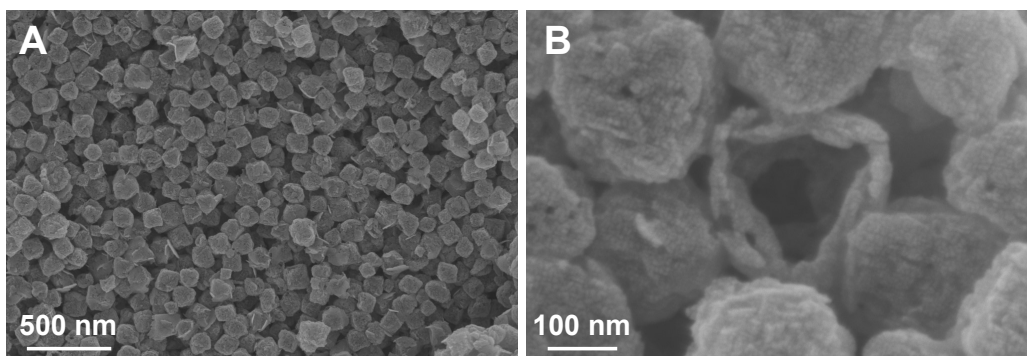


**Figure S1** (A) and (B) SEM images of  $\text{Cu}_7\text{S}_4$  nanoparticles.

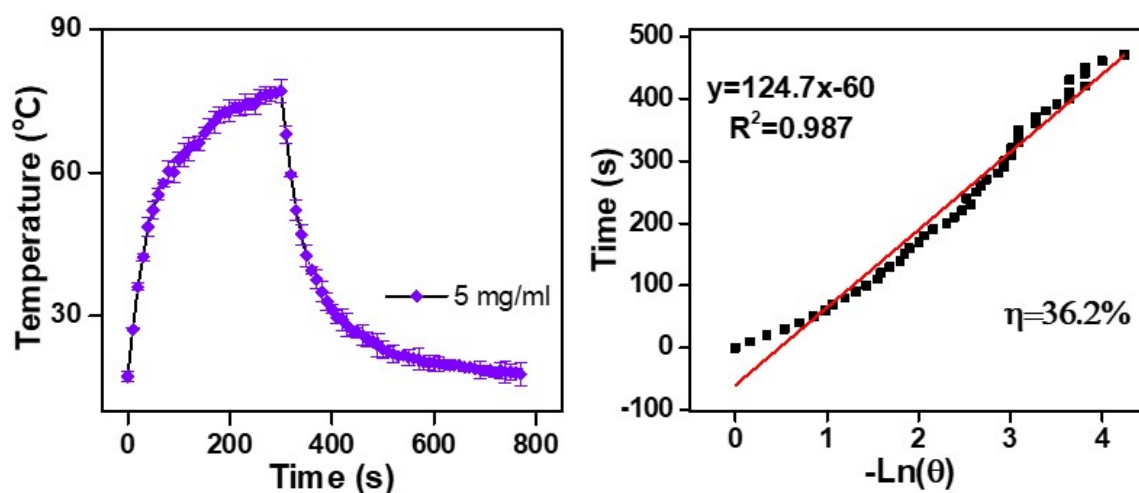


**Figure S2** (A) Temperature profile of aqueous modified  $\text{Cu}_7\text{S}_4$  solution irradiated with 980 nm laser at  $1 \text{ W cm}^{-2}$  for 5 min and then cooled naturally after turning off the laser. (B) Heating-cooling curves recorded for aqueous modified  $\text{Cu}_7\text{S}_4$  solution under 980 nm laser irradiation according to the “Roper model” to obtain the photothermal conversion efficiency values-36.2%.

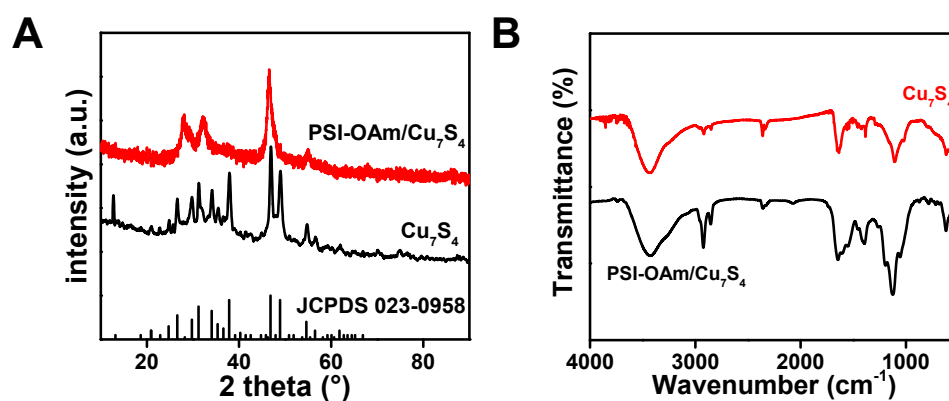


**Figure S3** (A) XRD of  $\text{Cu}_7\text{S}_4$  and aqueous modified  $\text{Cu}_7\text{S}_4$ . (B) IR spectrum of  $\text{Cu}_7\text{S}_4$  and aqueous modified  $\text{Cu}_7\text{S}_4$ .

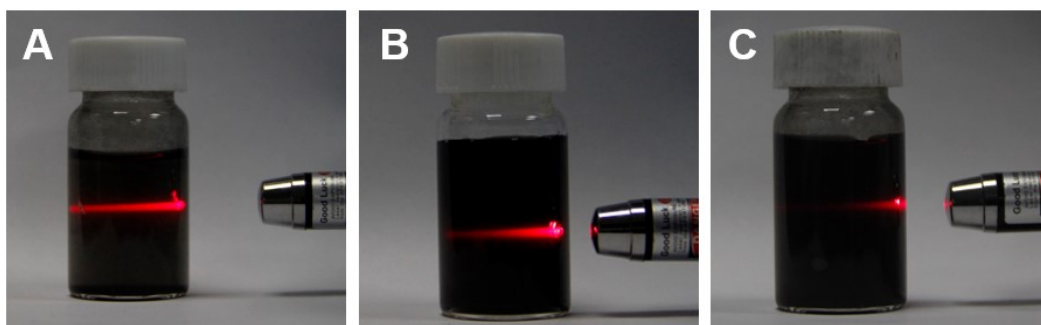


**Figure S4** Tindal effect corresponding to different concentrations of  $\text{Cu}_7\text{S}_4$  nanoparticles doping amounts of 0.1 wt% (A), 0.3 wt%(B), 0.4 wt% (C), respectively.

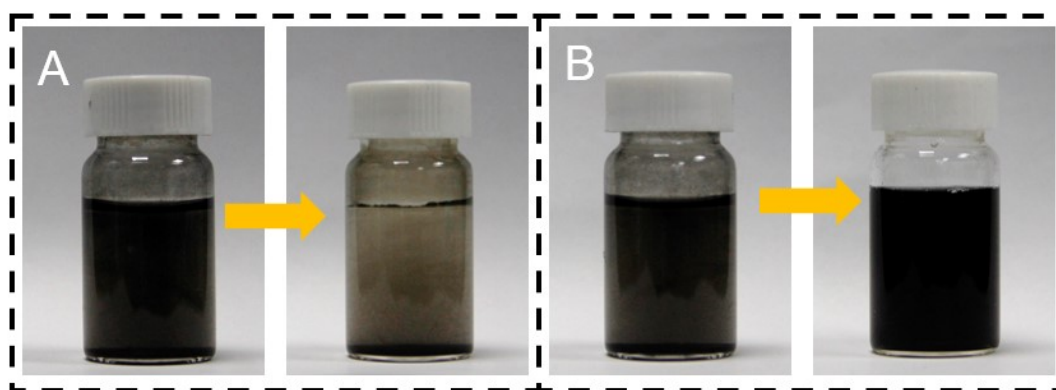


**Figure S5** (A) The unmodified  $\text{Cu}_7\text{S}_4$  nanoparticles (0.2 wt%) were slowly deposited on the bottom of the bottle after being dispersed in the silicone sol for a period of time. (B) The aqueous modified  $\text{Cu}_7\text{S}_4$  nanoparticles (0.2 wt%) dispersed in the organosilicon sol remained well dispersed in the colloidal state for more than one week after resting.

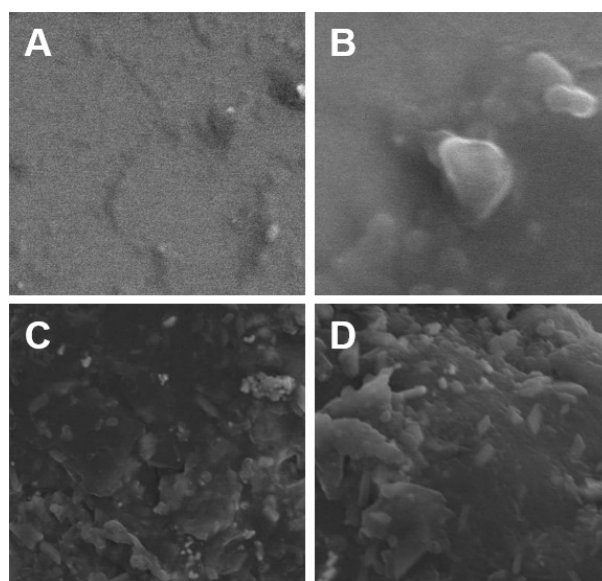


**Figure S6** SEM images of the coating surface corresponding to different hydrolysis times of 1

h (A), 2 h (B), 4 h (C), and 5 h (D), respectively.

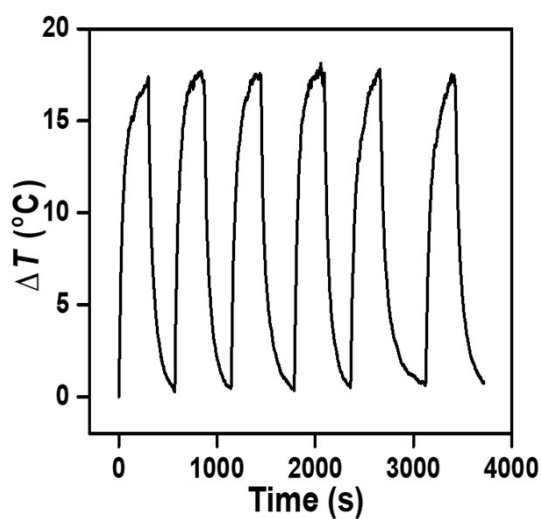


**Figure S7** Photothermal cycle stability testing of coated glass.

**Table S1.** Research progress on transparent anti-icing coatings.

Materials	CA (°)	Transmittance	Self-heating capacity	Ref.
Bio-based epoxy resin	107	81%	--	1
POSSPDMAEMA- <i>b</i> -P SBMA	105	85%	--	2
Titanate nanotubes	117	57%	--	3
Silicone sol	105	77%	--	4
Titania	171	48%	--	5
Silica nanoparticles	--	60%	--	6
Liquid-infused coating	101	82%	--	7
ITO	--	90%	Electric heating	8
Cu <sub>7</sub> S <sub>4</sub> /organo-silicone sol	121.8	≥75%	Photothermal	This work

**Supplementary note:**

Table S1 compares the recent research works on transparent anti-icing coatings in the past years. Generally, transparent anti-icing coatings are designed by doping hydrophobic nanoparticles ( $\text{SiO}_2$ ,  $\text{TiO}_2$ , etc.) into the transparent coating directly, however, the excessive doping leads to a decrease in the overall transmittance of the coating. Our designed coating achieves a better balance between transmittance and hydrophobicity compared with previous work. At the same time, due to the doping of photothermal conversion nanoparticles, the self-heating function under light conditions also gives the coating a better anti-/de-icing melting property.

**Table S2.** Adhesion test results of different samples

Sample number	Doping amount of PU	Treatment conditions	Thickness	Adhesion rating
1	0%	110 °C/1 h	5 $\mu\text{m}$	3
2	1%	110 °C/1 h	5 $\mu\text{m}$	1
3	2%	110 °C/1 h	5 $\mu\text{m}$	1
4	3%	110 °C/1 h	5 $\mu\text{m}$	2
5	4%	110 °C/1 h	5 $\mu\text{m}$	2
6	5%	110 °C/1 h	5 $\mu\text{m}$	3
7	1%	110 °C/0.5 h	5 $\mu\text{m}$	3
8	1%	110 °C /1.5 h	5 $\mu\text{m}$	1
9	1%	110 °C /2 h	5 $\mu\text{m}$	1
10	100%	110 °C/1 h	--	5
11	1%	110 °C/1 h	15 $\mu\text{m}$	2
12	1%	110 °C/1 h	28 $\mu\text{m}$	4
13	1%	110 °C/1 h	34 $\mu\text{m}$	5

**Supplementary note:**

The adhesion reflects the durability performance of the coating in application. The effect of different factors on the adhesion of the coating was tested and the results are shown in Table S2 (The adhesion strength gradually decreases in the order from 0 to 5). Firstly, we compared the effects of different waterborne PU doping amounts on the adhesion of the coating. When the doping amount is 0%, the viscosity of the silicone sol is low, though the annealing treatment can increase the bonding between the coating and the substrate, it cannot ensure the continuous integrity of the coating, so the adhesion strength of the coating is low. This problem can be effectively improved by doping with aqueous PU doping, which shows excellent adhesion between the coating and the glass when the PU doping amount is 1% and 2%, while with the increase of PU doping, it will affect the bonding between the silicone sol and the glass, which leads to the decrease of the coating adhesion. In addition, we also tested the adhesion of water-based PU on the glass surface, the results show that the adhesion rating of PU on the glass surface is only 5. Secondly, the annealing time also significantly affects the adhesion of the coating, when the annealing time is lower than 1h, the insufficient bonding between the coating and the glass substrate also leads to the decrease of the adhesion of the coating, and the adhesion between the coating and the glass reaches the highest when the annealing time exceeds 1h. The effect of annealing temperature on coating adhesion is similar to that of annealing time. The increase in annealing temperature promotes bonding between the coating and the glass, thus improving adhesion. Finally, different thicknesses of the coating were tested and the results showed that the adhesion strength of the coating decreased significantly with the increase of the coating thickness. In general, the best performance of coating adhesion was achieved when the PU doping amount reached 1%, the coating thickness was 5  $\mu\text{m}$ , and the annealing time and annealing temperature were 1h and 110  $^{\circ}\text{C}$ , respectively.

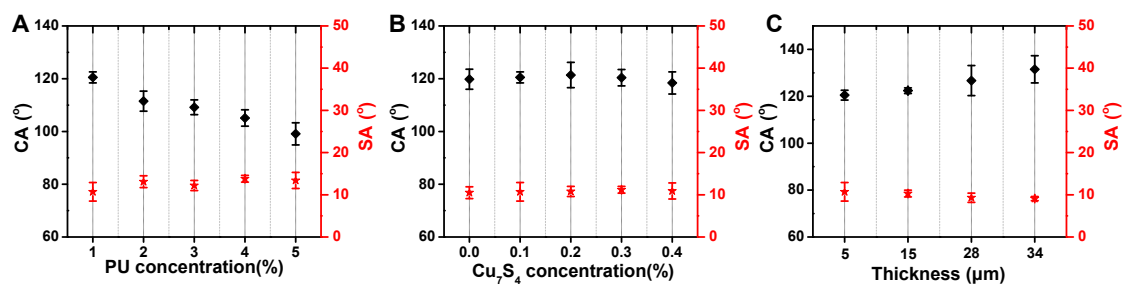


**Figure S8** CA and SA of the coating with (A) different PU concentration, (B) different  $\text{Cu}_7\text{S}_4$  concentration and (C) different thickness, respectively.

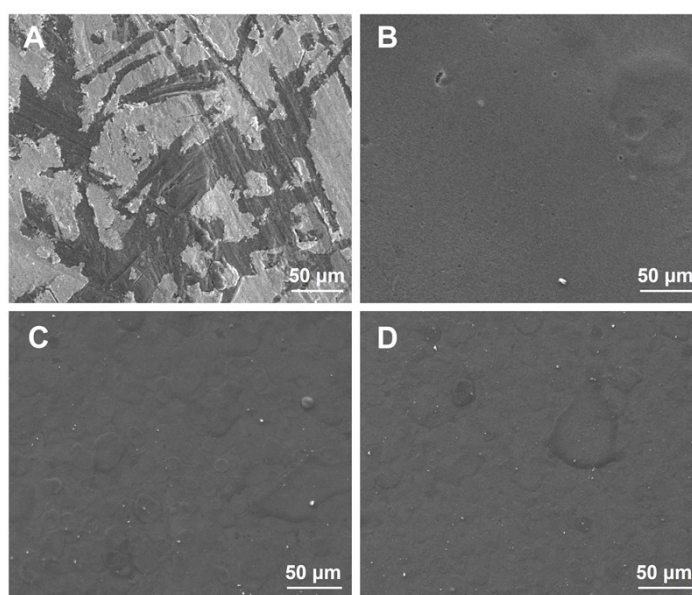


**Figure S9** SEM of the coating with different PU concentration (A) 0%, (B) 2%, (C) 3%, (D) 4%, respectively.

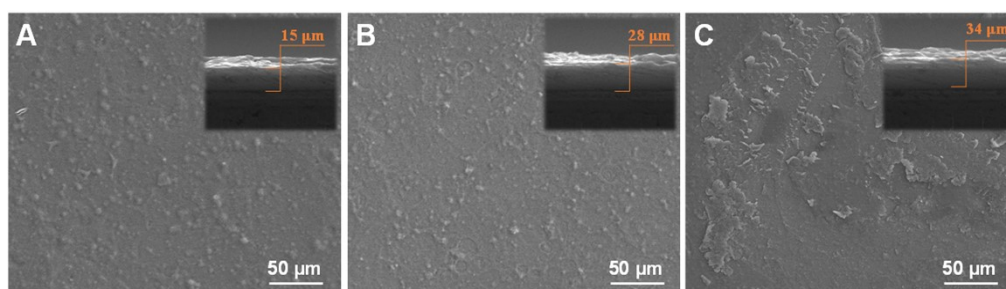


**Figure S10** SEM of the coating with different thickness (A) 15  $\mu\text{m}$ , (B) 28  $\mu\text{m}$ , (C) 34  $\mu\text{m}$ , respectively.

**Supplementary note:**

The coating surface without PU doping was prone to flaking after undergoing annealing due to the surface tension, but too much PU doping tended to form blocks of PU on the coating surface, which was not conducive to the hydrophobicity of the coating (Fig. S8A, Fig. S9). And the doping amount of  $\text{Cu}_7\text{S}_4$  nanoparticles basically has no effect on the hydrophobicity of the coating (Fig. S8B). The SEM images (Fig. S10) with different coating thicknesses shows that the increase of coating thickness leads to the appearance of "fish scale" irregular structure on the coating surface, which enhanced the hydrophobicity of the coating (Fig. S8C).

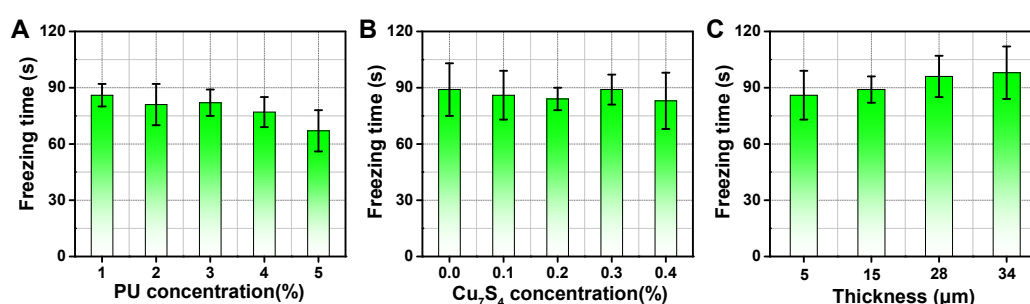


**Figure S11** Freezing time of 5 µL droplets under -20 °C with (A) different PU concentration, (B) different  $\text{Cu}_7\text{S}_4$  concentration and (C) different thickness, respectively.

#### Supplementary note:

The increase of PU concentration and coating thickness leads to shorter and longer freezing time of droplets, respectively (Fig. S11A, B). While the doping of nanoparticles has no significant effect on the freezing time of droplets (Fig. S11C).

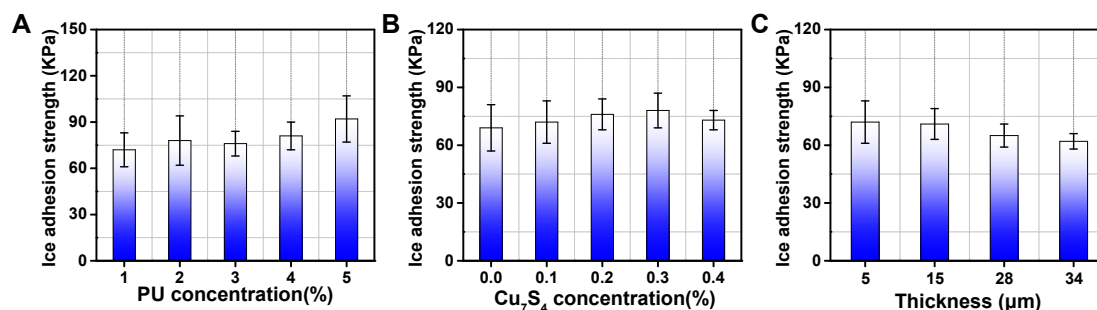


**Figure S12** Ice adhesion strength of the coating with (A) different PU concentration, (B) different  $\text{Cu}_7\text{S}_4$  concentration and (C) different thickness, respectively.

### Supplementary note:

The ice adhesion strength increases with the increase of PU doping (Fig. S11A), and the ice adhesion strength reaches the highest when the nanoparticles reach 0.3% of the doping amount, and decreases with the continued increase to 0.4% (Fig. S11B). Finally, the increase in the thickness of the coating significantly reduces the ice adhesion strength on the coating surface (Fig. S11C).

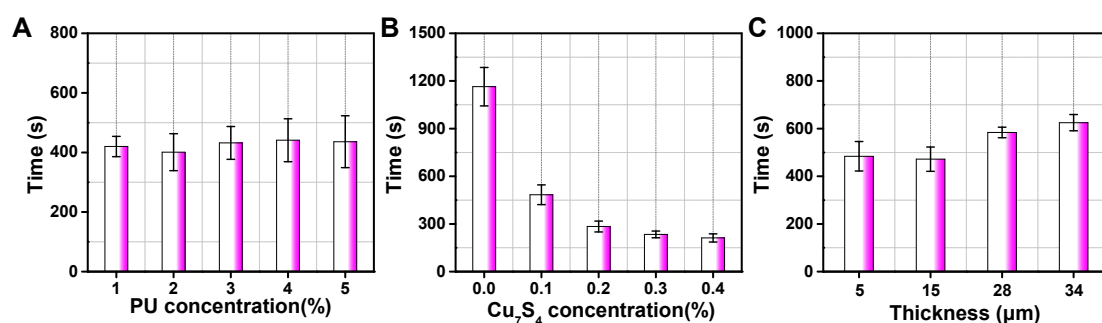


**Figure S13** De-icing time with (A) different PU concentration, (B) different Cu<sub>7</sub>S<sub>4</sub> concentration and (C) different thickness, respectively.

### Supplementary note:

With the increase of PU doping, the decrease of hydrophobicity slightly weakens the de-icing efficiency of the coating (Fig. S13A). And with the increase of the doping amount of photothermal conversion nanoparticles, the heating rate of the coating as well as the maximum temperature that can be reached will be significantly enhanced, which will improve the de-icing effect of the coating (Fig. S13B), and finally the increase of the coating thickness leads to the decrease of the photothermal conversion effect of the coating, which will reduce the de-icing rate of the coating (Fig. S13C).

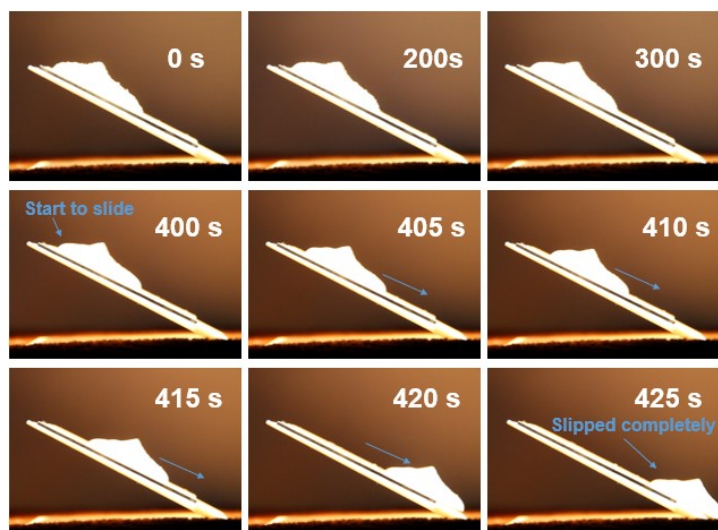


**Figure S14** The side views image sequences showing the deicing process under 1-sun illumination on the surface of coated glass.

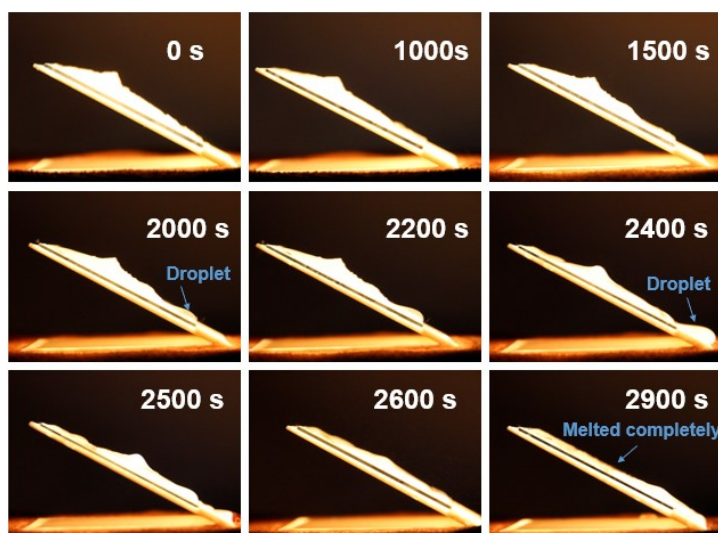


**Figure S15** Side views image sequences showing the deicing process under 1-sun illumination on the surface of blank glass.

### Reference

1. X. H. Wu, S. L. Zheng, D. A. Bellido-Aguilar, V. V. Silberschmidt, Z. Chen, *Mater. Design*, 2018, **140**, 516-523.
2. C. Li, X. H. Li, C. Tao, L. X. Ren, Y. H. Zhao, S. Bai, X. Y. Yuan, *ACS Appl. Mater. Inter.*, 2017, **9**, 22959-22969.
3. X. H. Wu, Y. X. Tang, V. V. Silberschmidt, P. Wilson, Z. Chen, *Adv. Mater. Inter.*, 2018,

- 5, 1800773-1800783.
4. X. H. Wu, Z. Chen, *J. Mater. Chem. A*, 2018, **6**, 16043-16053.
  5. S. H. Liu, M. Sakai, B. S. Liu, C. Terashima, K. Nakata, A. Fujishima, *RSC Adv.*, 2013, **3**, 22825-22830.
  6. B. Liang, Z.X. Zhong, E. Jia, G. Y. Zhang, Z. H. Su, *ACS Appl. Mater. Inter.*, 2019, **11**, 30300–30307.
  7. M. M. Liu, Y. Y. Hou, J. Li, L. Tie, Z. G. Guo, *Chem. Eng. J.*, 2018, **337**, 462–470.
  8. K. Im, K. Cho, J. Kim, S. Kim, *Thin Solid Films*, 2010, **518**, 3960–3963.
  9. T. Hanas, K. T. S. Sampath, P., Govindaraj, D., Mukesh, *Mat. Sci. Eng. C-Mater.*, 2016, **65**, 43-50.
  10. L. Vast, J. Delhalle, Z. Mekhalif, *Int. J. Adhes. Adhes.*, 2009, **29**, 286-293.
  11. T. Hanas, K. T. S. Sampath, P., Govindaraj, D., Mukesh, R. Seeram, *J. Mater. Process Tech.*, 2018, **252**, 398-406.
  12. C. Song., Y. X. Yang, Y. F. Zhou, L. G. Wang, S. J. Zhu, J. F. Wang, *Mater. Lett.*, 2019, **252**, 202-206.
  13. S. Ferdinand, S. Magdalena, M. Caroline, H. Sarah, V. Sannakaisa, *ACS Appl. Mater. Inter.*, 2015, **7**, 26758-26766.
  14. Y. Z. Shen, Y. Wu, J. Tao, C. L. Zhu, H. F. Chen, Z. W. Wu, Y. H. Xie, *ACS Appl. Mater. Inter.*, 2019, **11**, 3590-3598.
  15. Y. Tian, K. Guo, X. F. Bian, T. Q. Wang, S. H. Chen, *Surf. Coat. Tech.*, 2017, **328**, 444–450.